J. Fluid Mech. (1988), *vol.* 189, *pp.* 397–421
Printed in Great Britain

Viscous oscillations of a supported drop in an immiscible fluid

By M. STRANI AND F. SABETTA
Dipartimento di Meccanica e Aeronautica, Universita' di Roma 'La Sapienza', Rome, Italy

(Received 2 June 1986 and in revised form 21 May 1987)

The small-amplitude free vibrations of a spherical drop immersed in an outer immiscible fluid and in partial contact with a solid support are considered when both fluids are assumed to be viscous and incompressible, while gravity effects are neglected. Using the normal-mode decomposition and the Green-function method, the solution of the linearized Navier–Stokes equations is reduced to the solution of an eigenvalue problem. The model includes as particular cases the viscous model for a free drop proposed by Prosperetti (1980) and the inviscid model for a supported drop previously proposed by the authors.

The influence of the viscosity and of the support size are analysed both for the bubble and for the drop. At large values of the viscosity, the free drop shows significant differences with respect to the unsupported drop and a singular behaviour of the eigenvalue problem as the support size tends to zero.

The comparison with the available experimental data shows a quite satisfactory agreement for both the vibration frequency and the damping constant, provided that the support angle is not too large.

1. Introduction

The study of drop vibrations in a zero-gravity environment is relevant to the technology of crystal growth in space laboratories. This led to the selection of the drop-vibration problem as one of the experiments to be performed during the Spacelab 1 flight in 1984. The experiment, named ES326, was carried out within the Physics of Fluids Modulus by the astronauts Merbolt and Lichtenberger who observed the resonance frequencies and the decay of vibrations for drops of various sizes supported on a solid disk. The results of this experiment, which have been described in detail by Rodot & Bisch (1984), compared favourably with those obtained from simulations on Earth using the Plateau technique of two immiscible fluids having equal density (Bisch, Lasek & Rodot 1982).

Beside the Earth and space experimental investigations, the drop-vibration problem can also be studied on a theoretical basis. However the existing investigations on the vibrations of drops immersed in an outer fluid (e.g. Miller & Scriven 1968; Prosperetti 1980; Marston 1980; Tsamopoulos & Brown 1983) are not suitable for crystal-growth problems where the drop cannot be considered to be isolated. A more appropriate model is the one adopted in the experimental investigation by Bisch *et al.* (1982) who modelled the crystallizing liquid as a drop lying on a plane solid support that represents the crystallized substratum. A slightly different model in which the plane support was substituted by a spherical bowl has been assumed by the authors in a previous study concerned with the inviscid

problem (Strani & Sabetta 1984). The spherical-support assumption, although clearly convenient for the mathematical modelling of the problem, is more restrictive than the flat support assumption since it requires the drop radius to be exactly the same as the bowl radius. However some *ad hoc* experimental investigations kindly performed by Dr C. Bisch have shown a negligible influence of the support shape on the vibration-frequency values. Using a spherical and a cylindrical support with the same support angle ψ_0 (see figure 1), exactly the same value of the first vibration frequency has been obtained for values of ψ_0 up to 90°. For larger values of the support angle ($\psi_0 = 127°$ and 156°) the vibration frequency using the spherical support was 10% larger than that measured with the plane support. Since support angles larger than 90° are not of practical interest and since the spherical shape is clearly convenient for the mathematical treatment of the problem, the spherical support will also be adopted in the present model.

In their study of the inviscid problem Strani & Sabetta (1984) showed that the effect of the support is to raise considerably the values of the resonance frequencies. Moreover for the supported drop a new lower-frequency free mode was observed, which reduces to a zero-frequency rigid displacement in the case of a free drop. In the above-mentioned work a comparison between the theoretical and the experimental data obtained by Bisch *et al.* (1982) was also presented, showing a quite good qualitative agreement. However the computed values of the frequencies were larger by about 20% than the experimental ones.

The aim of the present work is to investigate if these differences were due to the inviscid assumption, looking for a solution of the supported-drop problem when both the internal and external fluid are considered to be viscous. Moreover the present model allows the determination on a theoretical basis of the decay of the drop vibrations.

In §2, using the normal-mode decomposition proposed by Miller & Scriven (1968) and Prosperetti (1980) for a free viscous drop, and the results obtained by Strani & Sabetta (1984) for an inviscid supported drop, the solution of the linearized Navier–Stokes equations is reduced to the solution of a characteristic value problem, which is very similar to the eigenvalue problem except that the coefficient matrix depends on the eigenvalue itself. The behaviour of the solution in the limiting cases of zero viscosity and the absence of the support is considered in §3.

In §4, the numerical method of solution of the eigenvalue problem is described, and a first set of results is presented for the case of a bubble and a drop. These results, when compared with those for the free drop, show an interesting singular behaviour of the eigenvalue problem as the support angle goes to zero.

Finally in §5 our numerical results are compared with the experimental ones obtained by various authors from simulations on Earth and with those obtained during the Spacelab 1 flight in 1984.

2. The mathematical model

2.1. *Formulation of the problem*

We consider the small-amplitude free vibrations of a spherical drop, partially supported by a bowl (figure 1), immersed in an immiscible fluid. Both the internal and the external fluid are assumed to be viscous and incompressible, while gravity effects are neglected. When a spherical polar coordinate system (r, θ, ϕ) is adopted,

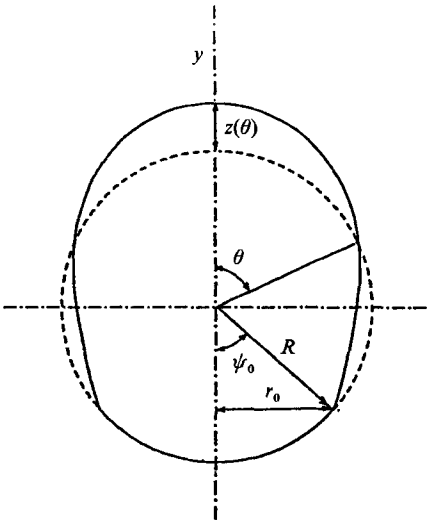

FIGURE 1. Definition sketch.

and only symmetrical deformations of the drop with respect to the y-axis are considered, the velocity and vorticity flow field may be written as:

$$\boldsymbol{V}(r,\theta,t) = V_r(r,\theta,t)\,\boldsymbol{n}_r + V_\theta(r,\theta,t)\,\boldsymbol{n}_\theta, \tag{1}$$

$$\boldsymbol{\Omega}(r,\theta,t) = \boldsymbol{\nabla}\times\boldsymbol{V} = \Omega(r,\theta,t)\,\boldsymbol{n}_\phi, \tag{2}$$

$$\Omega(r,\theta,t) = \frac{1}{r}[(rV_\theta)_{,r} - V_{r,\theta}], \tag{3}$$

where $\boldsymbol{n}_r, \boldsymbol{n}_\theta, \boldsymbol{n}_\phi$ are the unit vectors of the coordinate system. Here and in what follows the quantities pertaining to the internal or external fluid are denoted by the superscripts i and o, respectively. The absence of the superscript indicates that a statement is applicable to both fluids.

For all the quantities, a time dependence is assumed of the type

$$F(r,\theta,t) = f(r,\theta)\,\mathrm{e}^{-\gamma t},$$

where f and γ are complex numbers. The eigenvalue spectrum for the present problem is characterized by the conditions

$$\mathrm{Re}\,(\gamma) \geqslant 0, \tag{4a}$$

$$\mathrm{Im}\,(\gamma) \geqslant 0, \tag{4b}$$

where (4a) is induced on physical grounds while (4b) follows from the symmetry of the spectrum with respect to the real axis. It should be pointed out that we do not consider the continuous spectrum that may be obtained when the values of γ are assumed to be purely real, as shown by Prosperetti (1980).

In the above-mentioned hypotheses, both the flow fields defined on the domains $\mathscr{D}^{\mathrm{i}} \equiv ((r,\theta): 0 \leqslant r \leqslant R, 0 \leqslant \theta \leqslant \pi)$ and $\mathscr{D}^{\mathrm{o}} \equiv ((r,\theta): R \leqslant r \leqslant \infty, 0 \leqslant \theta \leqslant \pi)$ may be described by the set of linearized Navier–Stokes equations

$$\boldsymbol{\nabla}\cdot\boldsymbol{v} = 0, \tag{5}$$

$$\rho\gamma\boldsymbol{\omega} = \mu\boldsymbol{\nabla}\times\boldsymbol{\nabla}\times\boldsymbol{\omega}, \tag{6a}$$

$$\boldsymbol{\omega} = \boldsymbol{\nabla}\times\boldsymbol{v} \tag{6b}$$

associated with the following set of boundary conditions:

(i) continuity of normal and tangential velocity on the whole drop surface $0 \leqslant \theta \leqslant \pi$

$$v_r^{\mathrm{i}}(R,\theta) = v_r^{\mathrm{o}}(R,\theta) = -\gamma z(\theta), \tag{7}$$

$$v_\theta^{\mathrm{i}}(R,\theta) = v_\theta^{\mathrm{o}}(R,\theta), \tag{8}$$

where $z(\theta)$ is the surface displacement with respect to the unperturbed, spherical shape;

(ii) Continuity of tangential stresses and balance of the normal momentum on the free portion of the drop surface $0 \leqslant \theta \leqslant \theta_0$

$$S_{r\theta}^{\mathrm{i}}(R,\theta) = S_{r\theta}^{\mathrm{o}}(R,\theta), \tag{9}$$

$$S_{rr}^{\mathrm{i}}(R,\theta) - S_{rr}^{\mathrm{o}}(R,\theta) = \sigma\left\{\frac{2}{R} - \frac{1}{R^2}\left[\frac{1}{\sin\theta}(\sin\theta z_{,\theta})_{,\theta} + 2z\right]\right\}, \tag{10}$$

where

$$S_{r\theta} = \mu\left[\frac{v_{r,\theta}}{r} + r\left(\frac{v_\theta}{r}\right)_{,r}\right],$$

$$S_{rr} = -p + 2\mu v_{r,r};$$

(iii) no-slip condition and no radial deformation on the supported portion of the drop surface $\theta_0 \leqslant \theta \leqslant \pi$

$$v_\theta(R,\theta) = 0, \tag{11}$$

$$z(\theta) = 0. \tag{12}$$

Moreover the following integral condition expresses the conservation of the drop volume

$$\int_0^\pi z \sin\theta \,\mathrm{d}\theta = 0. \tag{13}$$

In the above equations ρ and μ are the density and the coefficient of viscosity of the fluids, σ is the surface tension, R the unperturbed drop radius and $\theta_0 = \pi - \psi_0$ where ψ_0 is the support angle (see figure 1). Boundedness of velocity and pressure at the origin and at infinity is also required.

Equations (5)–(13) determine an eigenvalue problem which is reduced, in the following, to a simpler form in order to allow for the use of an efficient approximate numerical method of solution.

2.2. *The solution for inner and outer flow fields*

Use is made here of the standard (Morse & Feshbach 1953) decomposition of a solenoidal vector $\boldsymbol{\omega}$,

$$\boldsymbol{\omega} = \nabla \times (\boldsymbol{B} + \nabla \times \boldsymbol{C}) \quad \text{with} \quad \boldsymbol{B} = B\boldsymbol{n}_r, \quad \boldsymbol{C} = C\boldsymbol{n}_r, \tag{14}$$

previously used by Miller & Scriven (1968) and Propseretti (1980) for the case of a free drop.

Since we only consider axisymmetric vibrations, it follows that $\boldsymbol{C} = 0, \boldsymbol{B} = B(r,\theta)\boldsymbol{n}_r$ and, consequently,

$$\boldsymbol{v} = \boldsymbol{B} + \nabla\phi \quad \text{with} \quad \phi = \phi(r,\theta). \tag{15}$$

The substitution of (15) into (6*a*) gives the following differential equation for the vector potential B:

$$-\frac{\rho\gamma}{\mu} B_{,x} = B_{,rrx} + \frac{[(1-x^2)B_{,x}]_{,xx}}{r^2}, \tag{16}$$

which admits separable solution in the form

$$B_n = \mathscr{B}_{n+\frac{1}{2}}\left[r\left(\frac{\rho\gamma}{\mu}\right)^{\frac{1}{2}}\right]P_n(x) \quad (n = 0, 1, 2, \ldots).$$

Here $x = \cos\theta$, $\mathscr{B}_{n+\frac{1}{2}}$ is a particular solution of the Bessel equation of semi-integer order, and $P_n(x)$ is the Legendre polynomial of order n. Since $(P_n(x))$ is a basis for $L_2[-1, 1]$ and the boundary conditions are given on spherical boundaries we may assume the following formal representation for the solution of (16):

$$B^{\mathrm{i}} = \sum_{n=1}^{\infty} T_n^{\mathrm{i}}(r)\,P_n(x) = \left(\frac{r^{\mathrm{i}}}{R^{\mathrm{i}}}\right)^{\frac{1}{2}} \sum_{n=1}^{\infty} C_n^{\mathrm{i}} \frac{J_{n+\frac{1}{2}}(r^{\mathrm{i}})}{J_{n+\frac{1}{2}}(R^{\mathrm{i}})} P_n(x), \tag{17a}$$

$$B^{\mathrm{o}} = \sum_{n=1}^{\infty} T_n^{\mathrm{o}}(r)\,P_n(x) = \left(\frac{r^{\mathrm{o}}}{R^{\mathrm{o}}}\right)^{\frac{1}{2}} \sum_{n=1}^{\infty} C_n^{\mathrm{o}} \frac{H^1_{n+\frac{1}{2}}(r^{\mathrm{o}})}{H^1_{n+\frac{1}{2}}(R^{\mathrm{o}})} P_n(x), \tag{17b}$$

where $r^{\mathrm{i,o}} = r[(\rho\gamma/\mu)^{\mathrm{i,o}}]^{\frac{1}{2}}$, $J_{n+\frac{1}{2}}$ and $H^1_{n+\frac{1}{2}}$ are respectively Bessel and Hankel functions of first kind and semi-integer order and $C_n^{\mathrm{i,o}}$ are constants. The particular choice of the Bessel functions for the inner and outer solution is due to the required boundedness condition on the velocity for $r \to 0$ and $r \to \infty$. The $n = 0$ term is not considered in the expressions since its curl would be identically zero.

The differential equation for the scalar potential ϕ is obtained by substituting (15) into (5):

$$\frac{1}{r^2}(r^2\phi_{,r})_{,r} + \frac{1}{r^2}[(1-x^2)\,\phi_{,x}]_{,x} = -\frac{1}{r^2}(r^2 B)_{,r}. \tag{18}$$

Introducing the expansion

$$\phi(r, x) = \sum_{n=0}^{\infty} \phi_n(z)\,P_n(x), \tag{19}$$

on account of (17) and of the boundedness conditions for $r \to 0$ and $r \to \infty$, it is found that

$$\phi_n^{\mathrm{i}} = \left(\alpha_n - \frac{n+1}{2n+1}\int_R^r s^{-n} T_n^{\mathrm{i}}(s)\,\mathrm{d}s\right) r^n - \left(\frac{n}{2n+1}\int_0^r s^{n+1} T_n^{\mathrm{i}}(s)\,\mathrm{d}s\right) r^{-(n+1)}, \tag{20}$$

$$\phi_n^{\mathrm{o}} = \left(\frac{n+1}{2n+1}\int_r^{\infty} s^{-n} T_n^{\mathrm{o}}(s)\,\mathrm{d}s\right) r^n + \left(\beta_n - \frac{n}{2n+1}\int_R^r s^{n+1} T_n^{\mathrm{o}}(s)\,\mathrm{d}s\right) r^{-(n+1)}, \tag{21}$$

where $T_0^{\mathrm{i}}(s) = T_0^{\mathrm{o}}(s) = 0$ and α_n, β_n are constants.

Finally for the drop shape we assume the expansion

$$z(x) = \sum_{n=1}^{\infty} z_n P_n(x), \tag{22a}$$

$$z_n = \frac{\langle z, P_n\rangle}{\langle P_n, P_n\rangle} = \frac{2n+1}{2}\int_{-1}^{1} z(y)\,P_n(y)\,\mathrm{d}y, \tag{22b}$$

where the zeroth-order term has been dropped on account of (13). The boundary conditions (7), (8), (9) and (11) may now be used to express the unknown quantities $C_n^{\mathrm{i}}, C_n^{\mathrm{o}}, \alpha_n, \beta_n$ as functions of the coefficients z_n.

Since the conditions (7) and (8) are identical with the ones to be used in the absence of the solid support, the quantities $\beta_n, C_n^{\mathrm{i}}, C_n^{\mathrm{o}}$, have the same expressions as previously obtained by Prosperetti (1980). These expressions, as functions of α_n and z_n, are listed in the Appendix. The boundary conditions (9) and (11) determine a

linear relationship between the vectors (α_n) and (z_n) which may be written in the form

$$\frac{2n+1}{n+1}R^{(n-1)}\alpha_n = \sum_{m=1}^{\infty} B_{nm}\frac{\gamma z_m}{m+1}. \tag{23}$$

The algebraic details to obtain the expressions of the coefficients $B_{n\,m}$ are also given in the Appendix.

All the constants needed to determine the inner and outer bulk flow field are now expressed in terms of α_0 and of the set $(z_n), n = 1, 2, \ldots$. The difference between the normal stresses at the drop surface is then given, up to a constant $(p^{\mathrm{o}}-p^{\mathrm{i}})$, by

$$(S^{\mathrm{i}}_{rr}-S^{\mathrm{o}}_{rr})_{|\mathrm{R}} = (p^{\mathrm{o}}-p^{\mathrm{i}})-\rho^{\mathrm{i}}\gamma\alpha_0+\rho^*\gamma^2 R\sum_{n,\,m=1}^{\infty}\Gamma_{nm}z_m P_n(x), \tag{24}$$

$$\Gamma_{nm} = \frac{1}{\rho^*}\left\{\left(\frac{\rho^{\mathrm{i}}}{n}+\frac{\rho^{\mathrm{o}}}{n+1}\right)-\frac{1}{\gamma R^2}\left[\frac{\mu^{\mathrm{i}}(2n+1)}{n}\tilde{\mathscr{J}}_{n+\frac{3}{2}}(R^{\mathrm{i}})-2(\mu^{\mathrm{i}}-\mu^{\mathrm{o}})(n+2)\right]\delta_{nm}\right.$$
$$\left.+\frac{1}{\rho^*\gamma R^2}\frac{\mu^{\mathrm{o}}n\tilde{\mathscr{H}}_{n-\frac{1}{2}}(R^{\mathrm{o}})-\mu^{\mathrm{i}}(n+1)\tilde{\mathscr{J}}_{n+\frac{3}{2}}(R^{\mathrm{i}})+2(\mu^{\mathrm{i}}-\mu^{\mathrm{o}})n(n+1)}{m+1}B_{nm}\right\}, \tag{25}$$

where ρ^* is a reference density.

2.3. *The eigenvalue problem*

As shown by the authors for the case of the inviscid drop (Strani & Sabetta 1984), using the Green-function method, the surface deformation may be obtained in the form

$$z(x) = \int_{-1}^{1} G(x, y)\,f(y)\,\mathrm{d}y. \tag{26}$$

The algebraic details on the Green-function evaluation are given in the above-mentioned paper and the only difference is that the function $f(y)$ is now given by

$$f(y) = \left[\frac{2\sigma}{R}+S^{\mathrm{i}}_{rr}(R, y)-S^{\mathrm{o}}_{rr}(R, y)\right]\frac{R^2}{\sigma}. \tag{27}$$

However if we replace the constant α_0 by a new constant

$$\phi_0 = \frac{1}{\rho^*\gamma^2 R}\left[(p^{\mathrm{o}}-p^{\mathrm{i}})-\rho^{\mathrm{i}}\gamma\,\alpha_0+\frac{2\sigma}{R}\right], \tag{28}$$

using (23), the function $f(y)$ may be expressed exactly in the same form as obtained for the inviscid case, i.e.

$$f(y) = \frac{\rho^*\gamma^2 R^3}{\sigma}\left[\phi_0+\int_{-1}^{1}\Gamma(y, \tau)\,z(\tau)\,\mathrm{d}\tau\right], \tag{29}$$

where $\Gamma(y, \tau)$ is now defined as

$$\Gamma(y, \tau) = \sum_{n,\,m=1}^{\infty}\frac{2m+1}{2}\Gamma_{nm}P_n(y)\,P_m(\tau), \tag{30}$$

Following the procedure used in the paper by Strani & Sabetta (1984), it is then possible to evaluate the constant ϕ_0 and to finally get the solution in the form

$$-\frac{1}{\lambda^2} z_h = \sum_{l=1}^{\infty} K_{hl} z_l, \tag{31a}$$

where K_{hl} is now given by

$$K_{hl} = \sum_{n=1}^{\infty} \frac{2}{2n+1} \left(\frac{G_{h0} G_{n0}}{G_{00}} - G_{hn} \right) \Gamma_{nl} \tag{31b}$$

and

$$\lambda = \left(\frac{\rho^* \gamma^2 R^3}{\sigma} \right)^{\frac{1}{2}}. \tag{32}$$

In the following we shall refer to λ as the eigenvalue of the problem even if, in the usual sense, the eigenvalue would be $\lambda' = -1/\lambda^2$.

The main difference with respect to the inviscid case is that the matrix K_{hl} is now a function of the eigenvalue itself. The problem is therefore slightly different and more complicated than the classical eigenvalue problem. Beside the dependence on the non-dimensional eigenvalue λ, it is easily recognized that the matrix K_{hl} depends on the support parameter $a = \cos\theta_0$, on the non-dimensional densities and viscosities $\rho^i/\rho^*, \rho^o/\rho^*, \mu^i/\mu^*, \mu^o/\mu^*$, (with μ^* a reference viscosity) and on a non-dimensional viscosity parameter

$$\epsilon = \frac{\mu^*}{(\rho^* R \sigma)^{\frac{1}{2}}}. \tag{33}$$

3. Limit cases of the inviscid drop and of the free drop

For completeness we now discuss some asymptotic forms of (31).

On account of the following expansions for large values of the argument:

$$\tilde{\mathscr{J}}_{m+\frac{3}{2}}(z) \approx z \cot\left(z - \frac{m+1}{2} n \right) + \ldots \quad \text{as } |z| \to \infty,$$

$$\tilde{\mathscr{H}}_{m-\frac{1}{2}}(z) \approx -\mathrm{i}z + \ldots \quad \text{as } |z| \to \infty,$$

the reader may easily verify that, in the limit of small viscosities the inviscid case previously treated by Strani & Sabetta (1984) is recovered since $A_n \to 0$, $Z_n \to 0$, $B_{nm} \to -\delta_{nm}$ and

$$K_{hl} \to \left(\frac{G_{0l} G_{h0}}{G_{00}} - G_{lh} \right) \left(\frac{\rho^i/\rho^*}{l} + \frac{\rho^o/\rho^*}{l+1} \right).$$

The viscous case of the free drop (Prosperetti 1980) is analogously found by taking the limit of (7) for $a \to -1$. In fact, when $a \to -1$

$$B_{nm} \to -\frac{Z_n}{A_n} \delta_{nm},$$

while (Strani & Sabetta 1984)

$$\lim_{a \to -1} G_{ik} = \frac{(2i+1)(2k+1)}{4} \frac{(-1)^k \frac{2\delta_{i1}}{3} + \frac{2\delta_{ik}}{2k+1}}{2 - k(k+1)}, \quad (i,k) \neq (1,1)$$

and G_{11} diverges as $\ln(1+a)$.

The matrix K_{hl} has an 'arrow shaped' structure, i.e.

$$\left.\begin{aligned}
&\lim_{a\to -1} K_{11} = \infty,\\
&\lim_{a\to -1} K_{1l} \neq 0, \quad l \neq 1\\
&\lim_{a\to -1} K_{h1} \neq 0, \quad h \neq 1\\
&\lim_{a\to -1} K_{hl} = 0, \quad h \neq l, \quad h,l \neq 1\\
&\lim_{a\to -1} K_{mm} = \frac{1}{m(m+1)-2}\left\{\left(\frac{\rho^{\mathrm{i}}/\rho^*}{m}+\frac{\rho^{\mathrm{o}}/\rho^*}{m+1}\right)-\frac{1}{\rho^*\gamma R^2}\right.\\
&\qquad\times\left[\left(\frac{2m+1}{m}\mu^{\mathrm{i}}\tilde{\mathscr{J}}_{m+\frac{3}{2}}(R^{\mathrm{i}})-2(m+2)(\mu^{\mathrm{i}}-\mu^{\mathrm{o}})\right)\right.\\
&\qquad\left.\left.\times\left(1-\frac{(m/(m+1))\,\mu^{\mathrm{o}}\tilde{\mathscr{H}}_{m-\frac{1}{2}}(R^{\mathrm{i}})-\mu^{\mathrm{i}}\tilde{\mathscr{J}}_{m+\frac{3}{2}}(R^{\mathrm{i}})+2m(\mu^{\mathrm{i}}-\mu^{\mathrm{o}})}{2(\mu^{\mathrm{i}}-\mu^{\mathrm{o}})-(\mu^{\mathrm{i}}\tilde{\mathscr{J}}_{m+\frac{3}{2}}(R^{\mathrm{i}})+\mu^{\mathrm{o}}\tilde{\mathscr{H}}_{m-\frac{1}{2}}(R^{\mathrm{o}})}\right)\right]\right\}, \quad m \neq 1.
\end{aligned}\right\} \tag{34}$$

Therefore in the limit case of a free drop the eigenvalues and eigenvectors have the following asymptotic behaviour:

$$\lambda^1 \to 0, \qquad Z_k^1 \to \delta_{1k}, \tag{35a}$$

$$\lambda^n \to -K_{nn}^{-\frac{1}{2}}(\lambda^n), \quad Z_k^n \to \delta_{nk}. \tag{35b}$$

As for the inviscid supported drop the existence of a first eigenmode which tends to a rigid displacement for $a \to -1$ is demonstrated: furthermore (35*b*) is identical with the nonlinear equation used by Prosperetti for the determination of λ^n when $n \neq 1$.

4. Numerical solution of the eigenvalue problem

The eigenvalue problem (31) may be numerically solved, as is usually done, by truncating the expansions to N terms (typical values used in the calculations were $N = 10, 20, 30$), and finding the roots of the characteristic equation

$$\det\left[\frac{1}{\lambda^2}\boldsymbol{U}_N + \boldsymbol{K}_N(\lambda, \epsilon, a)\right] = 0, \tag{36}$$

where $\boldsymbol{U}_N$ is the identity $N \times N$ matrix, $\boldsymbol{K}_N$ is the $N \times N$ truncation of the infinite matrix K_{hl} in (31), and the non-dimensional values of densities and viscosities are assumed to be given. The nonlinear eigenvalue problem (36) has been solved iteratively by a Newton–Ralphson procedure. The solution is very sensitive to the initial guess of the value $\lambda^n(\epsilon)$ and it may often occur that the solution diverges or converges to an eigenvalue different from the one sought (i.e. with different n). To avoid this difficulty the value $\lambda^n(\epsilon_0 - \Delta\epsilon)$ was used as initial guess to compute $\lambda^n(\epsilon_0)$. Starting from $\epsilon = 0$ where the eigenvalues are known (Strani & Sabetta 1984) and successively increasing ϵ by small steps $\Delta\epsilon$, the whole function $\lambda^n(\epsilon)$ has been built up. For the larger values of ϵ where $|\mathrm{d}\lambda/\mathrm{d}\epsilon|$ is greater, we could avoid the use of very small values of $\Delta\epsilon$ by giving to $\lambda(\epsilon_0)$ an initial approximate value obtained with a linear extrapolation from the values at $(\epsilon_0 - \Delta\epsilon)$ and at $(\epsilon_0 - 2\Delta\epsilon)$.

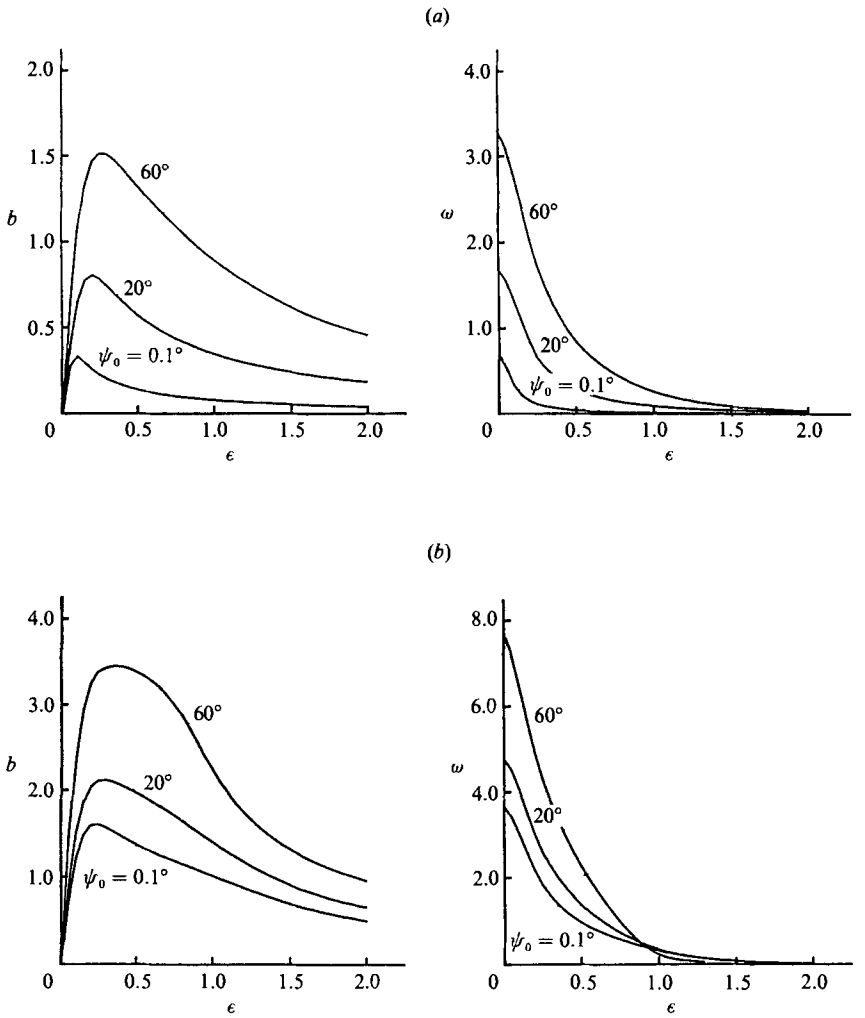

FIGURE 2. (*a*) First and (*b*) second eigenvalue $\lambda = b + i\omega$ versus ϵ for the bubble ($\mu^i = \rho^i = 0$) and different support angles ψ_0. Truncation $N = 10$.

4.1. *The bubble* [$\rho^i \equiv \mu^i = 0$]: *numerical results*

Plots versus ϵ of the real and imaginary part ($\lambda = b + i\omega$) of the first two eigenvalues are given in figure 2. It is seen that both the damping and the frequency of the oscillations increase with the angle of support, without modifications of their qualitative dependence on the viscosity. Decreasing ψ_0 for a given ϵ, the eigenvalues regularly approach the values predicted by the theory for $\psi_0 = 0$.

4.2. *The drop* [$\rho^o = \mu^o = 0$]: *numerical results*

Figure 3 shows the plot versus ϵ of the real and imaginary part of the first and second eigenvalue. As for the bubble case, an increase of b and ω with the support angle may be observed in the range of low ϵ-values. However for large values of ϵ, the second eigenvalue shows an irregular behaviour which is particularly evident for small values of the support angle. Moreover the solution for $\psi_0 = 0.1$ looks quite different from that for the unsupported drop, despite the fact that the latter is the limit of the solution as ψ_0 tends to zero (see §3).

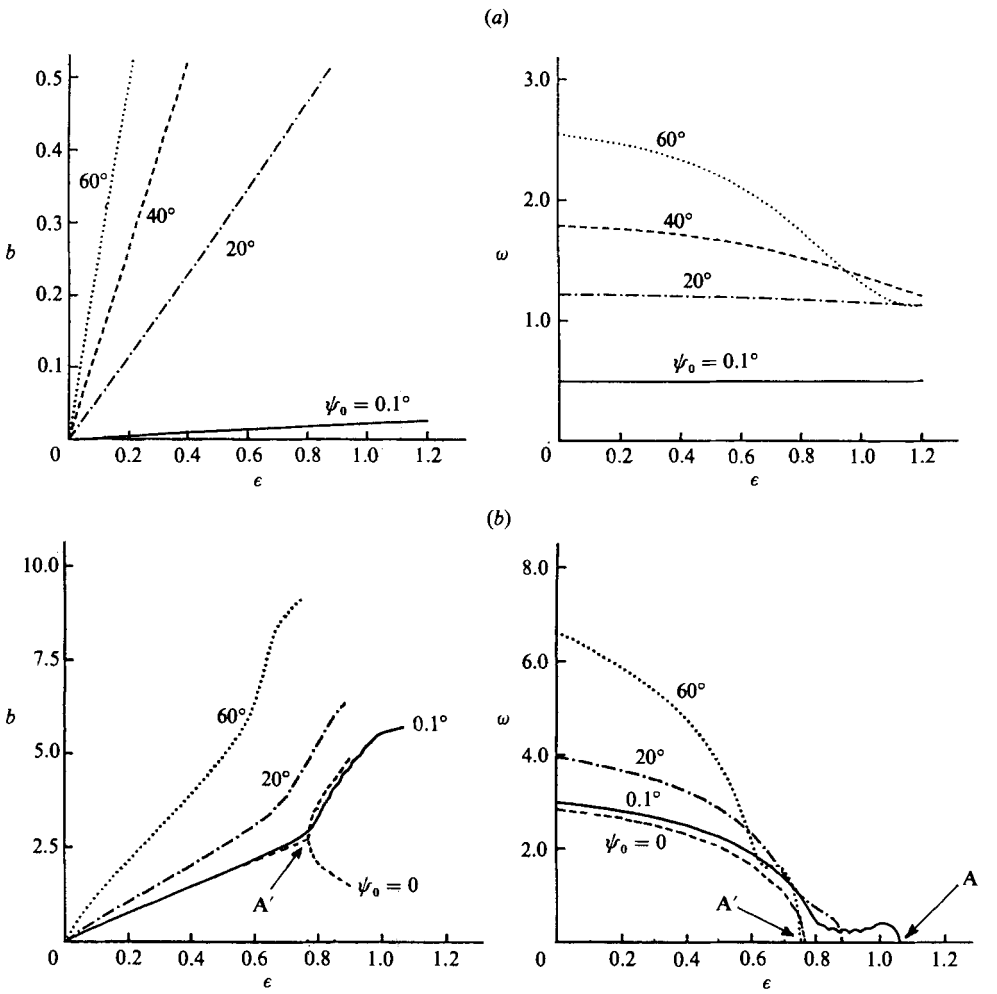

FIGURE 3. (*a*) First and (*b*) second eigenvalue $\lambda = b + \mathrm{i}\omega$ versus ϵ, for the drop ($\mu^o = \rho^o = 0$) and different support angles ψ_0. Truncation $N = 10$.

Before discussing this behaviour it is worth remembering that for the free drop the eigenmodes coincide with the Legendre polynomials and may then be identified by a number which is equal both to the order of the polynomial and to the number of nodes of the free-surface shape. For the supported drop we may still identify an eigenmode by the node number, but the same eigenmode, which is now a combination of different Legendre polynomials, may correspond to different positions of the nodes, depending on the relative weight of the Legendre polynomials.

In order to gain a better insight into the behaviour of the supported drop it is helpful to examine the complete picture of the roots of the characteristic equation, which is shown in figure 4 for the case of $\psi_0 = 0.1$ and a truncation number $N = 10$. From the analysis of this figure we may point out the following unexpected features:

(i) For the second eigenvalue the bifurcation point (point A in figure 4) has moved further with respect to the position of the bifurcation point for $\psi_0 = 0.1$ (point A′ in figure 3). Moreover while in the latter case the bifurcation gives rise to two purely real branches, both corresponding to a second eigenmode, the lower of the two

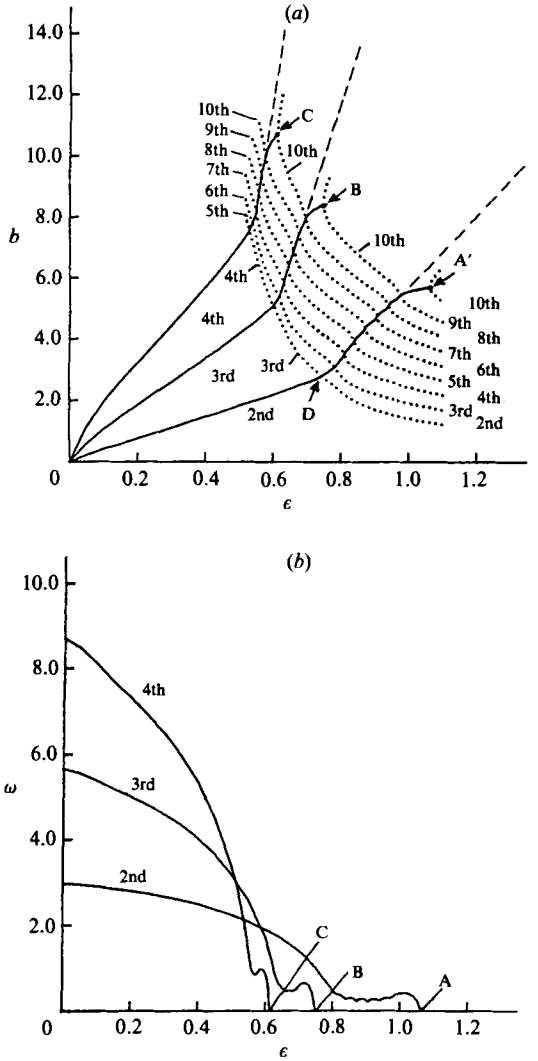

FIGURE 4. Roots $\lambda = b + i\omega$ of the characteristic equation for $\psi_0 = 0.1$ and truncation $N = 10$: ——, $\omega \neq 0$; · · · · · ·, $\omega = 0$. The ordinal number marked near each branch indicates the type of the corresponding eigenmode.

branches issuing from point A corresponds to a tenth eigenmode, i.e. to the highest mode that can be represented with $N = 10$. It should also be observed that point D in figure 4(*a*), even if quite similar to point A′, is not a bifurcation point, since the two crossing lines have different imaginary parts.

(ii) Along the purely real branches of the solution the mode number varies as shown in figure 4(*a*), i.e. in different ranges of ϵ the same real eigenvalue corresponds to different modes.

(iii) Both the real and the imaginary part of the second eigenvalue show some wiggles. The wiggles tend to disappear for the higher eigenvalues and for larger support angles.

All these features could suggest the occurrence of spurious solutions due to the finite truncation. To ascertain if this was the cause, an analysis of the influence of the truncation number on the second eigenvalue has been performed.

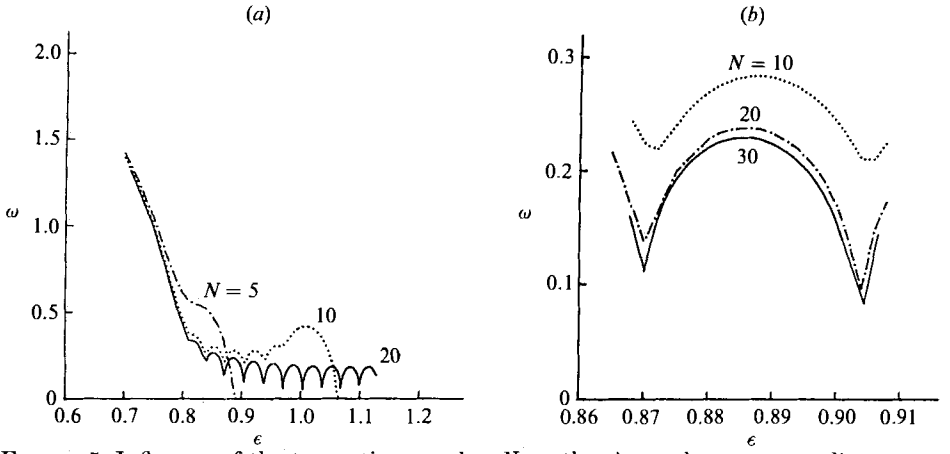

FIGURE 5. Influence of the truncation number N on the eigenvalue corresponding to a second mode for the drop. The real parts of the eigenvalues are not plotted. (*a*) $\psi_0 = 0.1$, (*b*) 0.5.

As shown in figure 5(*a*), if we increase the truncation number from $N = 5$ up to $N = 10$, the bifurcation point moves from $\epsilon = 0.89$ to $\epsilon = 1.065$. The comparison of the two solutions also shows that below a certain critical value $\epsilon^* \approx 0.78$ only a slight increase in the accuracy is obtained with $N = 10$, while for $\epsilon > \epsilon^*$ the two solutions are drastically different. A further increase in N (from 10 to 20) causes the bifurcation point to move even farther and the critical value to increase up to $\epsilon^* \approx 0.94$. An analogous behaviour could be observed for the real part of the solution. For instance with $N = 20$ a plot of the solution, like that of figure 4(*a*), would show the following modifications: the bifurcation points A, B, C would move to larger ϵ- and b-values and the solid lines would extend farther (approximately along the dashed lines); new dotted lines corresponding to eigenmodes larger than the 10th would appear in the upper part of the diagram; the solution would be modified only in the neighbourhood of points A, B, C while the lower part of the diagram would remain substantially unchanged.

From the above analysis we may draw the following conclusions:

(*a*) The appearance of points like A, B, C in figure 4 does not correspond to actual bifurcations but is caused by the finite truncation.

(*b*) For each eigenvalue and each value of the truncation number, a converged solution can be obtained only for ϵ-values below a critical value ϵ^*. To extend the solution above this value a larger N is needed.

(*c*) In the limit $N \to \infty$ the solution does not have the bifurcation points that exist for $\psi = 0$ but it is made up of two infinite sets of branches both extending in the whole range $0 < \epsilon < \infty$. The first set is constituted by branches with $\omega \neq 0$ and $\mathrm{d}b/\mathrm{d}\epsilon > 0$ along which the mode number is constant (solid lines in figure 4*a*); the second set is constituted by purely real branches with $\mathrm{d}b/\mathrm{d}\epsilon < 0$ (dotted lines in figure 4*a*) along which an iterated transition from an nth mode to an $(n-1)$th mode is observed.

The way by which the transition occurs is illustrated in figure 6 for the neighbourhood of point D of figure 4(*a*). The result seems to indicate that the non-oscillating way by which a perturbed drop may come back to its spherical shape is different according to the viscosity variation during this process. If the viscosity is kept constant, only the perturbation amplitude will gradually be reduced and the shape will remain the same. On the other hand if the viscosity is increased during the

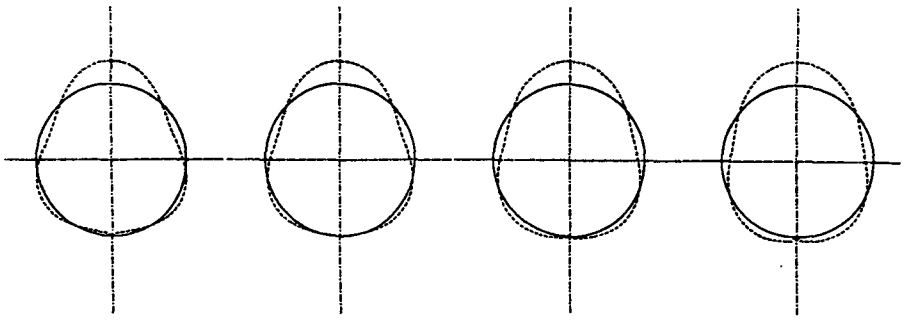

FIGURE 6. Transition from 3rd to 2nd eigenmode along a purely real branch.

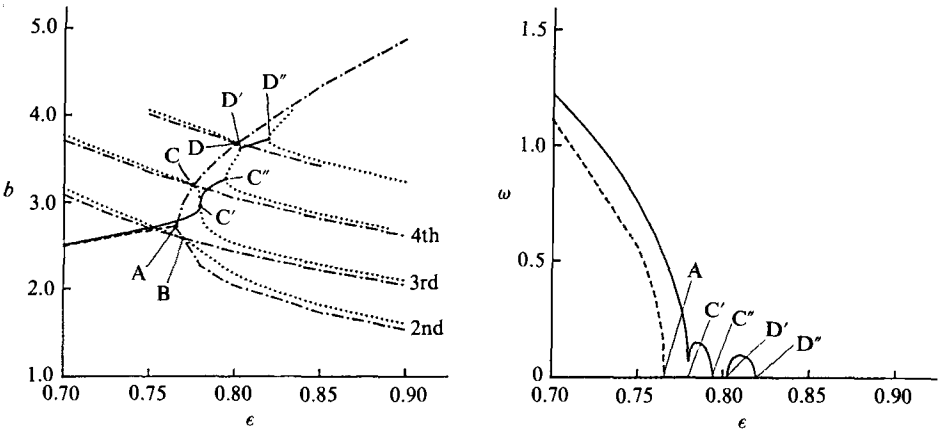

FIGURE 7. Comparison between solution curves of the eigenvalue problem for $\psi_0 = 0$ (– – –, $\omega \neq 0$; — · —, $\omega = 0$) and for $\psi_0 = 10^{-6}$ (——, $\omega \neq 0$; · · · · ·, $\omega = 0$).

process, the surface shape will become gradually smoother with a reduction in the number of the nodes. This behaviour, whose experimental validation would be valuable, is strictly connected with the presence of the support. In fact for the supported drop, an eigenmode is a combination of different Legendre polynomials having as weight the eigenvector components. Since the ratio of these components is affected by the viscosity, it is not surprising that an eigenvalue could correspond to different modes as the viscosity is changed.

Coming now to the problem of the wiggles, figure 5 shows that when N is increased from 10 to 20 the wiggle amplitude is strengthened instead of smoothed and that for $N = 30$ the wiggles seem to converge to a shape independent of N. We are therefore led to deduce that the wiggles are not due to the finite truncation, even if we are not able to give a physical interpretation of these oscillations. It is however possible to gain a better insight into the origin and the successive disappearance of the wiggles as ψ_0 is increased, through a comparison between the cases $\psi_0 = 0$ and $\psi_0 = 10^{-6}$ (figure 7).

For $\psi_0 = 0$ and, say, the second eigenvalue the complex solution bifurcates at point A into two purely real branches. The intersection of these branches with the decreasing purely real branches corresponding to higher modes gives rise to other bifurcation points like B, C, D in figure 7.

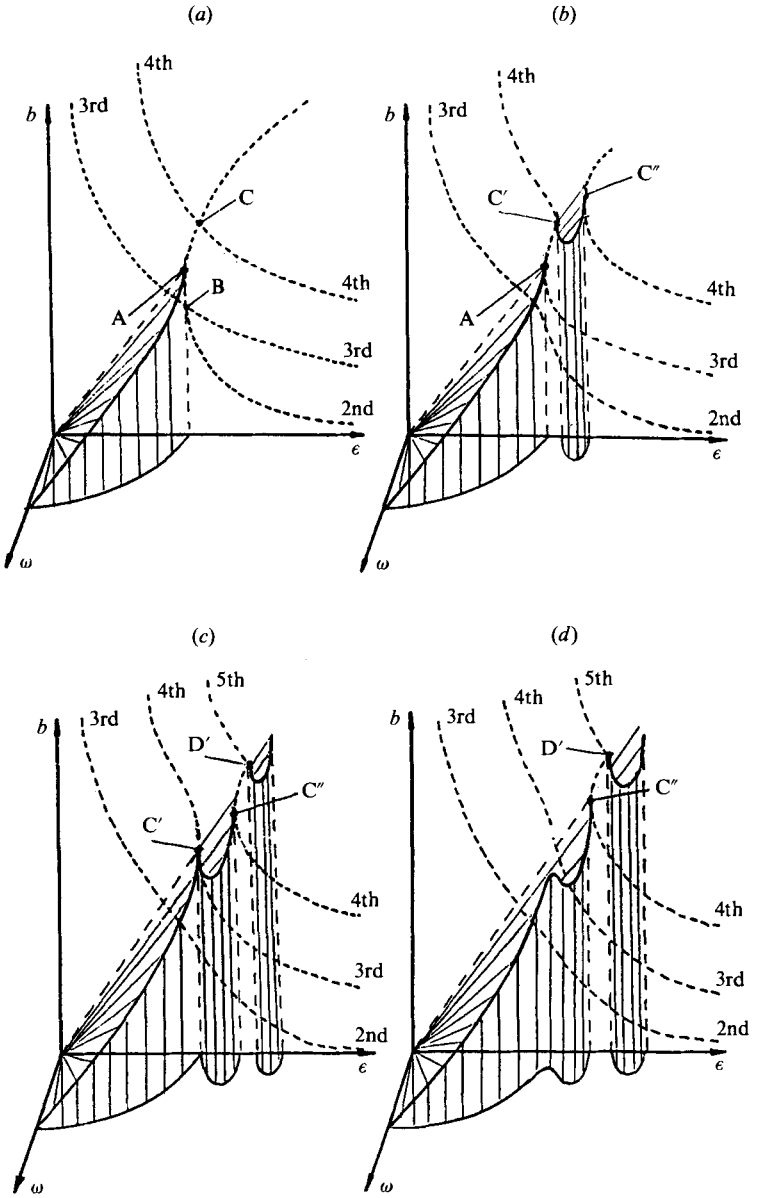

FIGURE 8. Qualitative plot of the dependence on ϵ of the eigenvalues $\lambda = b + i\omega$. The plot indicates the way the bifurcation points A, B, C... in (*a*) evolve and disappear with increasing ψ_0 (——, $\omega \neq 0$; – – –, $\omega = 0$).

The corresponding plot for $\psi_0 = 10^{-6}$, even if very close to the one for $\psi_0 = 0$, appears to be quite different and more complicated.

The three-dimensional plot of figure 8 qualitatively illustrates the way by which the transition occurs between $\psi_0 = 0$ (figure 8*a*) and $\psi_0 = 10^{-6}$ (figure 8*d*). As soon as $\psi_0 > 0$, the bifurcation point B disappears in the simple way shown in figure 8(*b*), while the point C splits up into two bifurcation points C′ and C″, which are connected by a complex branch. Further increases in ψ_0 cause the points A and C′ first to coalesce (figure 8*c*) and then to disappear (figure 8*d*), giving rise to a 'wiggle'. As ψ_0 is increased further, the wiggle becomes gradually smoother and finally vanishes.

In the same way we may observe the coalescence and then disappearance of points C″–D′, D″–E′ and so on for all the other bifurcation points.

The wiggles are thus seen to be intimately connected with the fact that all bifurcation points in the plot for $\psi_0 = 0$ must disappear when ψ_0 is increased and indicate a singular behaviour of the eigenvalue problem as the perturbation $(a+1)$ tends to zero.

5. Comparison with experimental data

We have summarized in table 1 the physical parameters characterizing the various sets of experimental data concerning both the frequencies (sets 1, 2, 4, 5, 10) and the damping constants (sets 3, 6, 7, 8, 9, 10). With the exception of set 10, which reports the data obtained in the Spacelab, all other results have been obtained in a laboratory simulation of the zero-gravity environment, using the Plateau technique of two immiscible fluids having equal density. Moreover sets 1, 2 and 3 are concerned with the small-amplitude vibrations of a free drop and therefore report data of the frequencies for $n \geqslant 2$ and of the damping constant for $n = 2$. On the other hand the remaining sets are concerned with the finite-amplitude vibrations of a supported drop and report results of the frequency and of the damping constant for $n = 1$.

The 110 different experimental conditions have been simulated using the present numerical model and the computed values are compared in figure 9 with the corresponding experimental values. The latters have been expressed in non-dimensional form through the relations

$$\omega_n = 2\pi F_n \left(\frac{\rho^* R^3}{\sigma}\right)^{\frac{1}{2}}, \quad b_n = \frac{1}{\tau_n}\left(\frac{\rho^* R^3}{\sigma}\right)^{\frac{1}{2}},$$

where F_n is the frequency in Hz of the nth vibration mode and τ_n is the corresponding decay time. The reference values $\mu^* = 10^{-2}$ g/cm s, and $\rho^* = \rho^i$ g/cm^3 have been assumed.

The comparisons of figure 9 indicates an overall agreement, measured by the scatter from the 45° line, but also some significant differences between the experimental and computed values. A discussion of these differences is given in the following through the analysis of the influence of the various physical parameters.

5.1. *Frequency*

Viscosity dependence

As shown by Strani & Sabetta (1984), the non-viscous model slightly overpredicts the value of the fundamental vibration frequency ($n = 1$) in the range of small support angles. To evaluate the influence of the viscosity we have computed the frequency for the 28 test conditions of set 4 having $\psi_0 < 35°$. For the actual values of the parameter ϵ, which varies from one test to another ranging from 3×10^{-3} to 10^{-2}, we obtained a reduction of the frequency of about 6% with respect to the inviscid case. The agreement with the experimental data is therefore slightly improved and the difference between the computed and experimental values always lies within $\pm 10\%$.

For larger values of the support angle the influence of the viscosity becomes progressively smaller. The weak influence of the viscosity on the vibration frequency confirms the observation of Bisch *et al.* (1982) who claimed that, for viscosities in the range of practical interest, the frequency is almost independent of the viscosity values of both the internal and the external fluid.

Set	Number of tests	Reference	Internal fluid	ρ^i g/cm^3	ν^i cSt	External fluid	ρ^o	ν^o cSt	σ dyn/cm	R cm	ψ_0 degrees
1	3	Trinh *et al.* (1982)	Silicone/CCL_4	0.99	3.2	Distilled water	0.99	1.1	37	0.71–0.77	0
2	1	Trinh *et al.* (1982)	Phenetole	0.96	1.22	Water/methanol	0.96	1.8	16.5	0.71	0
3	23	Trinh *et al.* (1982)	Silicone/CCL_4	0.99	3.2 68.6	Distilled water	0.99	1.1	37	0.49–0.71	0
4	38	Bisch (1983, private communication)	Aniline	1.002	4.4	Water/Brh	1.002	1	5.85	0.12–1.9	3–62
5	19	Bisch (1983, private communication)	Silicone/CCL_4	1	5	Water	1	1.4	37	0.75–12.5	24–156
6	8	Bisch *et al.* (1982)	Silicone 5	0.92	5	Water/ethanole	0.92	3	7	0.5–1.5	11.5–48.6
7	4	Bisch *et al.* (1982)	Water/ethanole	0.92	3	Silicone 5	0.92	5	7	0.75–1.45	17.5–48.6
8	5	Bisch *et al.* (1982)	Silicone 10	0.94	10	Water/ethanole	0.94	3	14	0.6–1.55	17.5–48.6
9	5	Bisch *et al.* (1982)	Water/ethanole	0.94	3	Silicone 10	0.94	10	14	0.6–1.5	17.5–48.6
10	4	Rodot & Bisch (1984)	Silicone	0.92	5	Air	0	0	20	1.7–2.7	34–62

TABLE 1. Physical parameters characterizing the sets of experimental data

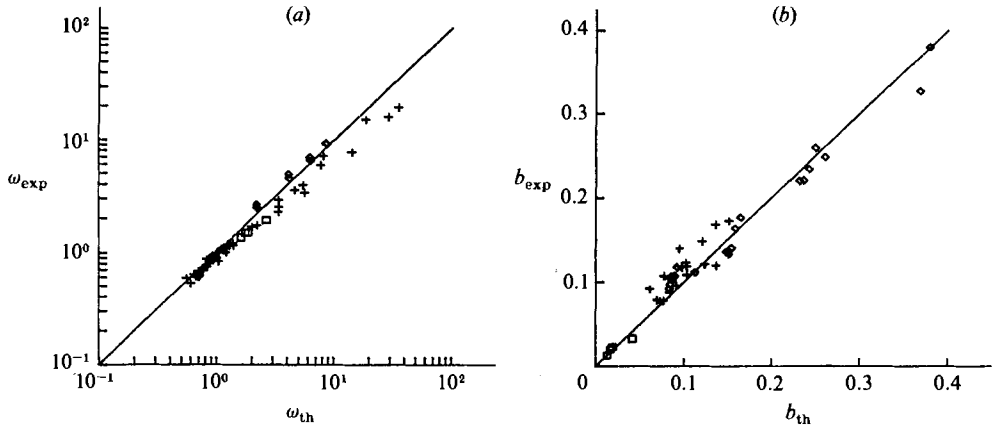

FIGURE 9. Comparison between experimental and computed eigenvalues. $\lambda = b + i\omega$. ◇, Trinh *et al.* (1982); +, Bisch *et al.* (1982); □, Spacelab experiment, Rodot & Bisch (1984).

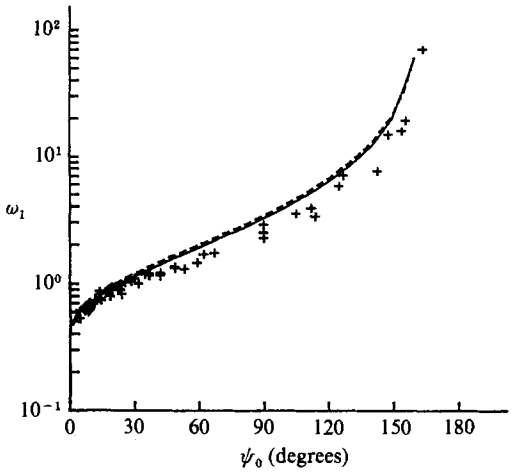

FIGURE 10. First free-mode frequency ω_1 versus the support angle. – – –, $\epsilon = 0$; ——, $\epsilon = 5 \times 10^{-2}$; +, Bisch (1983), private communication).

Support-angle dependence

The experimental values of the fundamental frequency over the whole range of the support angle are plotted in figure 10 and compared with the computed values for $\epsilon = 0$ and for $\epsilon = 0.5 \times 10^{-2}$, which represents an average of the test values. While the agreement is quite satisfactory for small support angles, both the inviscid and the viscous models overpredict the vibration frequency by almost 30% at $\psi_0 = 90°$ and by 80% at $\psi_0 = 150°$. This increasing disagreement as the support angle is increased may be connected with the nonlinear effects that are not taken into account in the model but that affect the experimental results by lowering the frequencies of the free modes as indicated by theoretical (Tsamopoulos & Brown 1983) and experimental (Trinh & Wang 1982) investigations. In fact, while for a free drop the vibration amplitude is characterized by the ratio between the pole displacement H and the drop radius, for a supported drop the significant parameter should be the ratio between H and a length characterizing the free portion of the drop, e.g. $R(\pi - \psi_0)$. Therefore it is clear that for the same values of H (as was the case in the experiments)

n	ω_{nL}	ω_n^*	Present model	Experimental set 1
2	2.19	2.12	2.12	2.46
3	4.14	4.00	3.99	4.49
4	6.32	6.09	6.07	6.48
5	8.73	8.51	8.36	9.06

TABLE 2. Comparison of calculated and experimental values of the frequency of free-drop oscillations

the nonlinear effects become more and more important as ψ_0 is increased. This interpretation of the disagreement for large support angles should however be supported by further *ad hoc* experimental investigations.

Higher-order modes

The only available results for $n > 1$ are those obtained for the free drop by Trinh, Zwern & Wang (1982). These results are compared in table 2 with the present model and with the non-dimensional frequencies for an inviscid free drop (Lamb 1932)

$$\omega_{nL} = \left[\frac{n(n+1)(n-1)(n+2)}{2n+1}\right]^{\frac{1}{2}}.$$

Table 2 also reports the values ω_n^* given by the expression

$$\omega_n^* = \omega_{nL} - \tfrac{1}{2}\delta\omega_{nL}^{\frac{1}{2}} + \tfrac{1}{4}\delta^2,$$

which takes into account a viscous correction. Here δ, in the case $\rho^i = \rho^o$, has the expression

$$\delta = (4R\rho^*\sigma)^{-\frac{1}{4}}[(\mu^i)^{-\frac{1}{2}} + (\mu^o)^{-\frac{1}{2}}]^{-1}(2n+1).$$

The computed values underpredict by 6%–13% the experimental ones, while they are almost coincident with the values of ω_n^*. However the fact that the experimental values are larger than Lamb's values, while the effect of viscosity is to lower the frequency values, seems to indicate that, in the present case, the differences between predicted and experimental values should be attributed to the uncertainty in the evaluation of the physical parameters (particularly the surface tension) and to the fact that a statically distorted drop (as it was in the above experiments) always has a resonance frequency larger than that for a spherical drop (Trinh *et al.* 1982).

5.2. *Damping constant*

Viscosity dependence

The influence of varying the viscosity of the inner fluid, all other parameters remaining constant, is shown in figure 11 for the case of a free drop. The agreement between the experimental damping constant and the model predictions is quite satisfactory. It may be observed that the agreement is much better than that indicated by Prosperetti (1980), who obtained differences between the observed and calculated decay times up to 150%.

Support-angle dependence

The lack of a set of experimental data in which only the support angle was varied, made it impossible a test of the model reliability over a wide range of ψ_0. However

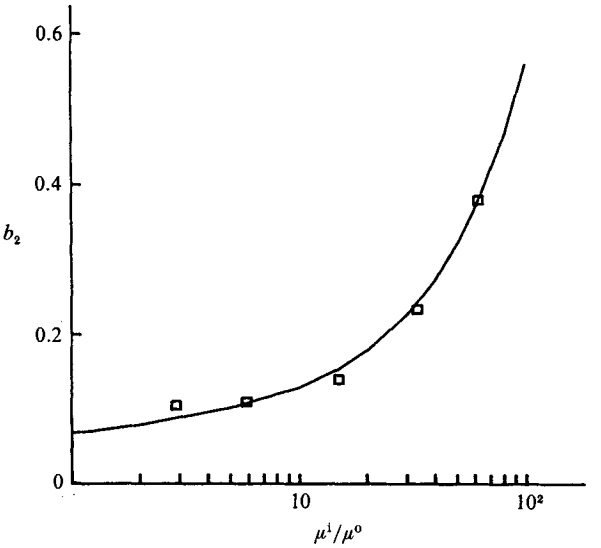

FIGURE 11. Influence of the viscosity ratio μ^i/μ^o on the damping constant ($n = 2, \psi_0 = 0$). ——, $\epsilon = 0.233 \times 10^{-2}$; □, Trinh *et al.* (1982).

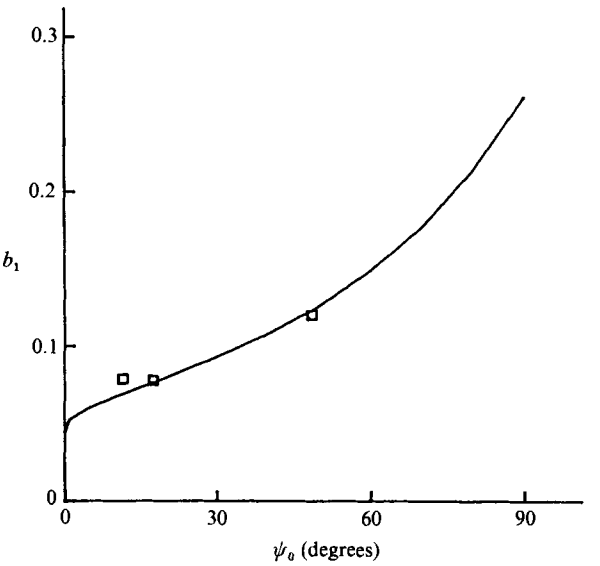

FIGURE 12. Influence on the damping constant of the support angle ($n = 1$). ——, $\epsilon = 0.39 \times 10^{-2}$; □, Bisch *et al.* (1982).

the few available data with constant ϵ compare favourably with the model predictions as shown in figure 12. The comparison for other combinations of the physical parameters and for values of ψ_0 up to 50° also shows that the agreement between experimental and computed values of the damping constant is better than that for the vibration frequency at large values of the support angle.

This behaviour is confirmed by the comparison shown in table 3 between the model predictions and the results obtained during the Spacelab 1 mission (Rodot & Bisch 1984).

ψ_0	R	ω_1		b_1	
degrees	cm	comp.	exp.	comp.	exp.
33.8	1.35	1.60	1.35	0.013	0.013
38.7	1.18	1.74	1.49	0.017	0.020
41.8	1.13	1.85	1.49	0.019	0.023
61.9	0.85	2.62	1.92	0.042	0.033

TABLE 3. Comparison between model predictions and the results of Rodot & Bisch (1984)

6. Conclusions

The model presented in this paper includes as particular cases the viscous model for a free drop proposed by Prosperetti (1980) and the inviscid model for a supported drop proposed by the authors (Strani & Sabetta 1984). The complexity and the computational effort of the model are not much larger than that of those mentioned above.

The model reliability is quite satisfactory for the prediction of both the vibration frequency and the damping constant, provided that the fundamental hypothesis of small-amplitude vibrations is satisfied.

The observed disagreement with experimental data for large values of the drop support angle is assumed to be due to the experimental large amplitude of the drop-pole displacement with respect to the free portion of the surface of the drop.

The authors wish to thank Professor G. M. Homsy for his suggestion of the solution of W. D. Collins of the dual series problem.

Professor Massimo Strani died before his time on September 12, 1986. The co-author wishes to remember the invaluable contribution of Massimo to the present work as well as to the understanding and the solution of a great deal of other fluid-dynamic problems. His death leaves a great gap among all his friends.

Appendix

The expressions for the constants β_n, C_n^{i} and C_n^{o} resulting from boundary conditions (7) and (8), are listed below (refer to the work of Prosperetti 1980 for a discussion and the algebraic details):

$$\left.\begin{aligned} \beta_0 &= 0, \\ \beta_n &= \frac{\gamma R^{(n+2)}}{n+1} z_n + \frac{n}{n+1} R^{(2n+1)} \alpha_n, \\ C_n^{\mathrm{i}} &= -\frac{2n+1}{n+1} \tilde{\mathscr{J}}_{n+\frac{1}{2}}(R^{\mathrm{i}}) \left(\frac{\gamma z_n}{n} + R^{(n+1)} \alpha_n \right), \\ C_n^{\mathrm{o}} &= \frac{2n+1}{n+1} \tilde{\mathscr{H}}_{n-\frac{1}{2}}(R^{\mathrm{o}})\, R^{(n-1)} \alpha_n. \end{aligned}\right\} \tag{A 1}$$

Here $$\tilde{\mathscr{J}}_\alpha(z) = \frac{zJ_{\alpha-1}(z)}{J_\alpha(z)}, \quad \tilde{\mathscr{H}}_\alpha = \frac{zH^1_{\alpha+1}(z)}{H^1_\alpha(z)}$$

are quotients of Bessel and Hankel functions.

If we remember that

$$v_r = B + \phi_{,r}, \quad v_\theta = \frac{\phi_{,\theta}}{r}, \quad S_{r\theta} = \mu\left[\frac{v_{r,\theta}}{r} + r\left(\frac{v_\theta}{r}\right)_{,r}\right]$$

the boundary conditions (9) and (11), on account of (17), (20) and (A 1) may be written as

$$\left.\begin{aligned}(S^{\mathrm{i}}_{r\theta} - S^{\mathrm{o}}_{r\theta})_{|r=R} &= (1-x^2)^{\frac{1}{2}} u_{,x} = -\frac{\mathrm{d}}{\mathrm{d}\theta}[u(\cos\theta)],\\ (v^{\mathrm{i}}_\theta)_{|r=R} &= (v^{\mathrm{o}}_\theta)_{|r=R} = (1-x^2)^{\frac{1}{2}} w_{,x} = -\frac{\mathrm{d}}{\mathrm{d}\theta}[w(\cos\theta)],\end{aligned}\right\} \tag{A 2}$$

where

$$\left.\begin{aligned} w(x) &= \alpha_0 + \sum_{n=1}^{\infty}\left(\frac{2n+1}{n+1}R^n\alpha_n + \frac{R}{n+1}\gamma z_n\right)P_n(x),\\ u(x) &= A_0\alpha_0 + \sum_{n=1}^{\infty}\left(A_n\frac{2n+1}{n+1}R^n\alpha_n + Z_n\frac{R}{n+1}\gamma z_n\right)P_n(x),\\ A_0 &= \frac{2}{1+\mu^{\mathrm{o}}/\mu^{\mathrm{i}}},\\ A_n &= \left[2(1-\mu^{\mathrm{o}}/\mu^{\mathrm{i}}) - \tilde{\mathscr{J}}_{n+\frac{3}{2}}(R^{\mathrm{i}}) - \frac{\mu^{\mathrm{o}}}{\mu^{\mathrm{i}}}\tilde{\mathscr{H}}_{n-\frac{1}{2}}(R^{\mathrm{o}})\right]\Big/\left(1+\frac{\mu^{\mathrm{o}}}{\mu^{\mathrm{i}}}\right),\\ Z_n &= \left[2(n+2)\left(1-\frac{\mu^{\mathrm{o}}}{\mu^{\mathrm{i}}}\right) - \frac{2n+1}{n}\tilde{\mathscr{J}}_{n+\frac{3}{2}}(R^{\mathrm{i}})\right]\Big/\left(1+\frac{\mu^{\mathrm{o}}}{\mu^{\mathrm{i}}}\right).\end{aligned}\right\} \tag{A 3}$$

With a change of variable $\psi = \pi - \theta$, (A 2) may be expressed in the form

$$\left.\begin{aligned}\sum_{k=0}^{\infty}(2k+3)\,x_k T^{-1}_{k+1}(\cos\psi) &= \sum_{m=0}^{\infty} Z_{m+1}R\gamma z_{m+1}(-1)^{m+1}\\ &\quad\times(m+1)\,T^{-1}_{m+1}(\cos\psi) = g(\psi), \quad \psi_0 < \psi < \pi,\\ \sum_{k=0}^{\infty}(1+H_k)\,x_k T^{-1}_{k+1}(\cos\psi) &= -\sum_{m=0}^{\infty} R\gamma z_{m+1}(-1)^{m+1}\\ &\quad\times(m+1)\,T^{-1}_{m+1}(\cos\psi) = f(\psi), \quad 0 < \psi < \psi_0,\end{aligned}\right\} \tag{A 4}$$

having defined

$$x_k = -(k+1)\,(-1)^{k+1}A_{k+1}R^{k+1}\alpha_{k+1}, \quad H_k = -\left(1+\frac{2k+3}{A_{k+1}}\right). \tag{A 5}$$

Differentiability term by term has been assumed, and account has been taken of the identity

$$(k+1)\,(k+2)\,T^{-1}_{k+1}(\cos\psi) = -\frac{\mathrm{d}}{\mathrm{d}\psi}P_{k+1}(\cos\psi), \tag{A 6}$$

where $T^{-1}_{k+1}(\cos\psi)$ are associated Legendre functions of degree $1+k$ and order -1.

The form (A 4) is a particular case of the dual series problem considered by Collins

(1961), whose solution is here synthetically recalled. The unknown coefficients x_k, solutions of (A 4), are found to be given by

$$\begin{aligned} x_k &= 2^{-\frac{1}{2}}\left\{\int_0^{\psi_0} I(\nu)\tan(\tfrac{1}{2}\nu)\sec(\tfrac{1}{2}\nu)[(k+1)\sin((k+2)\nu)+(k+2)\sin((k+1)\nu)]\,\mathrm{d}\nu\right. \\ &\quad \left.+\int_{\psi_0}^{\pi} G(\nu,\nu)\tan(\tfrac{1}{2}\nu)\sec(\tfrac{1}{2}\nu)[(k+1)\sin((k+2)\nu)+(k+2)\sin((k+1)\nu)]\,\mathrm{d}\nu\right\} \\ &= \pi(k+1)(k+2)\left[\int_0^{\psi_0} I(\nu)\,R^1_{1+k}(\nu)\,\mathrm{d}\nu+\int_{\psi_0}^{\pi} G(\nu,\nu)\,R^1_{1+k}(\nu)\,\mathrm{d}\nu\right] \\ &= \pi(k+1)(k+2)(a_k+b_k). \end{aligned} \tag{A 7}$$

The function $G(\nu,\sigma)$ is defined by

$$G(\nu,\sigma)=\frac{1}{2\pi}\int_{\sigma}^{\pi}\frac{g(\chi)\cot(\frac{1}{2}\chi)\sin\chi\,\mathrm{d}\chi}{(\cos\nu-\cos\chi)^{\frac{1}{2}}},\quad 0\leqslant\nu\leqslant\sigma, \tag{A 8}$$

while $I(\nu)$ must be found as a solution of the Fredholdm integral equation of the second kind

$$\begin{aligned} &\tan(\tfrac{1}{2}\nu)I(\nu)+\int_0^{\psi_0}K_1(\nu,\mu)\tan(\tfrac{1}{2}\mu)I(\mu)\,\mathrm{d}\mu \\ &=\frac{1}{\pi}\cot(\tfrac{1}{2}\nu)\frac{\mathrm{d}}{\mathrm{d}\nu}\int_0^{\nu}\frac{f(\chi)\tan(\frac{1}{2}\chi)\sin\chi\,\mathrm{d}\chi}{(\cos\chi-\cos\nu)^{\frac{1}{2}}}-\int_{\psi_0}^{\pi}K_1(\nu,\mu)\tan(\tfrac{1}{2}\mu)G(\mu,\mu)\,\mathrm{d}\mu,\quad 0<\nu<\psi_0, \end{aligned} \tag{A 9}$$

the Kernel $K_1(\nu,\mu)$ being given by

$$K_1(\nu,\mu)=\pi\cot(\tfrac{1}{2}\nu)\cot(\tfrac{1}{2}\mu)\sum_{k=0}^{\infty}(k+2)(k+1)H_k\,R^1_{1+k}(\nu)\,R^1_{1+k}(\mu), \tag{A 10}$$

with

$$R^1_{1+k}(\nu)=\frac{2^{-\frac{1}{2}}}{\pi}\sec(\tfrac{1}{2}\nu)\tan(\tfrac{1}{2}\nu)\left[\frac{\sin((k+1)\nu)}{(k+1)}+\frac{\sin((k+2)\nu)}{(k+2)}\right]. \tag{A 11}$$

The solution given by Collins is valid provided that H_k is $O(k^{-1})$ for large k.

For the present case

$$H_k=-1-\frac{2k}{A_{k+1}}-\frac{3}{A_{k+1}}.$$

If account is taken of the asymptotic expansions of the Bessel and Hankel functions for large order it is easily verified that

$$\lim_{k\to\infty}\frac{-2k}{A_{k+1}}=1,$$

from which the necessary condition on H_k immediately follows.

Since (A 4) is a linear problem, the solution x_k may be expressed as

$$x_k=\sum_{m=0}^{\infty}x_k^m(z_{m+1}R\gamma)(-1)^{m+1}, \tag{A 12}$$

where $x_k^m(k=0,1,2,\ldots)$ is the solution of (A 4) when

$$\begin{aligned} f(\psi)&=-(m+1)T^{-1}_{m+1}(\cos\psi), \\ g(\psi)&=Z_{m+1}(m+1)T^{-1}_{m+1}(\cos\psi). \end{aligned}$$

For this case we have

$$F(\nu) = \frac{1}{\pi}\cot(\tfrac{1}{2}\nu)\frac{\mathrm{d}}{\mathrm{d}\nu}\int_0^\nu \frac{f(\chi)\tan(\tfrac{1}{2}\chi)\sin(\chi)\,\mathrm{d}\chi}{(\cos\chi-\cos\nu)^{\frac{1}{2}}}$$

$$= -\frac{(m+1)}{\pi}\cot(\tfrac{1}{2}\nu)\frac{\mathrm{d}}{\mathrm{d}\nu}\int_0^\nu \frac{T_{m+1}^{-1}(\cos\chi)\tan(\tfrac{1}{2}\chi)\sin(\chi)\,\mathrm{d}\chi}{(\cos\chi-\cos\nu)^{\frac{1}{2}}}$$

and

$$G(\nu,\sigma) = \frac{1}{2\pi}\int_\sigma^\pi \frac{g(\chi)\cot(\tfrac{1}{2}\chi)\sin\chi\,\mathrm{d}\chi}{(\cos\nu-\cos\chi)^{\frac{1}{2}}} = \frac{(m+1)Z_{m+1}}{2\pi}\int_\sigma^\pi \frac{T_{m+1}^{-1}(\cos\chi)\cot(\tfrac{1}{2}\chi)\sin\chi\,\mathrm{d}\chi}{(\cos\nu-\cos\chi)^{\frac{1}{2}}}.$$

To evaluate the integrals we make use of the results (Collins 1961)

$$R_{1+m}^1(\nu) = \frac{1}{\pi}\frac{\mathrm{d}}{\mathrm{d}\nu}\int_0^\nu \frac{\sin\chi\tan(\tfrac{1}{2}\chi)T_{1+m}^{-1}(\cos\chi)\,\mathrm{d}\chi}{(\cos\chi-\cos\nu)^{\frac{1}{2}}} = \frac{-2^{\frac{1}{2}}\sin(\tfrac{1}{2}\nu)}{\pi(m+1)(m+2)}\frac{\mathrm{d}}{\mathrm{d}\nu}\left(\frac{\cos((m+\frac{3}{2})\nu)}{\cos(\frac{1}{2}\nu)}\right)$$

$$R_{1+m}^1(\pi-\mu) = \frac{(-1)^{m+1}}{\pi}\frac{\mathrm{d}}{\mathrm{d}\mu}\int_\mu^\pi \frac{\sin\chi\cot(\tfrac{1}{2}\chi)T_{1+m}^{-1}(\cos\chi)\,\mathrm{d}\chi}{(\cos\mu-\cos\chi)^{\frac{1}{2}}}$$

$$= \frac{2^{\frac{1}{2}}(-1)^{m+1}\cos(\tfrac{1}{2}\mu)}{\pi(m+1)(m+2)}\frac{\mathrm{d}}{\mathrm{d}\mu}\left(\frac{\sin((m+\frac{3}{2})\mu)}{\sin(\frac{1}{2}\mu)}\right),$$

from which it follows that

$$F(\nu) = -(m+1)\cot(\tfrac{1}{2}\nu)R_{1+m}^1(\nu), \tag{A 13}$$

and

$$\frac{\mathrm{d}G(\nu,\nu)}{\mathrm{d}\nu} = \frac{(-1)^{m+1)}(m+1)Z_{m+1}}{2}R_{1+m}^1(\pi-\nu)$$

$$= \frac{Z_{m+1}}{2^{\frac{1}{2}}\pi(m+2)}\cos(\tfrac{1}{2}\nu)\frac{\mathrm{d}}{\mathrm{d}\nu}\left(\frac{\sin((m+\frac{3}{2})\nu)}{\sin(\frac{1}{2}\nu)}\right),$$

whose integration, under the condition $G(\pi,\pi) = 0$, results in

$$G(\nu,\nu) = \frac{Z_{m+1}}{2^{\frac{1}{2}}\pi(m+2)}\left[\cot(\tfrac{1}{2}\nu)\sin((m+\tfrac{3}{2})\nu) - \frac{\cos((m+\frac{3}{2})\nu}{2m+3}\right]$$

$$= \frac{Z_{m+1}(m+1)}{(2m+3)}\cot^2(\tfrac{1}{2}\nu)R_{1+m}^1(\nu). \tag{A 14}$$

If we define

$$T_{hk}(\psi_0) = \int_0^{\psi_0}\cot^2(\tfrac{1}{2}\nu)R_{1+h}^1(\nu)R_{1+k}^1(\nu)\,\mathrm{d}\nu,$$

$$S_{hk}(\psi_0) = \int_{\psi_0}^\pi \cot^2(\tfrac{1}{2}\nu)R_{1+h}^1(\nu)R_{1+k}^1(\nu)\,\mathrm{d}\nu = \frac{\delta_{hk}}{\pi(h+2)(h+1)} - T_{hk}$$

we have

$$x_k^m = \pi(k+1)(k+2)(a_k^m + b_k^m),$$

with

$$b_k^m = \int_{\psi_0}^\pi G(\nu,\nu)R_{1+k}^1(\nu)\,\mathrm{d}\nu = \frac{Z_{m+1}(m+1)}{2m+3}\left(\frac{\delta_{km}}{\pi(k+2)(k+1)} - T_{km}\right)$$

while the multiplication of (A 9) by $R^1_{1+k}(\nu)/\tan(\frac{1}{2}\nu)$ and its integration between 0 and ψ_0, gives the infinite set of linear equations in the unknowns $a^m_k, k = 0, 1, 2, \ldots$:

$$\sum_{n=0}^{\infty} (\delta_{kn} + \pi(n+2)(n+1) H_n T_{kn}) a^m_n$$

$$= -(m+1)\left\{T_{mk}\left(1 + H_m \frac{Z_{m+1}}{2m+3}\right) - \pi \sum_{n=0}^{\infty} [(n+2)(n+1) H_n T_{kn} T_{nm}] \frac{Z_{m+1}}{2m+3}\right\}. \quad \text{(A 15)}$$

Setting

$$C_{kn} = (\delta_{kn} + \pi(n+1)(n+2) H_n T_{kn}),$$

$$v^m_k = T_{mk}\left(1 + H_m \frac{Z_{m+1}}{2m+3}\right) - \pi \sum_{n=0}^{\infty} [(n+1)(n+2) H_n T_{kn} T_{nm}] \frac{Z_{m+1}}{2m+3}$$

we get the formal solution of (A 15)

$$a^m_n = -(m+1) \sum_{k=0}^{\infty} C^{-1}_{nk} v^m_k = (m+1) D_{mn}. \quad \text{(A 16)}$$

This leads to the linear relation between the vectors $\{\alpha_n\}$ and $\{z_m\}$

$$\frac{2n+1}{n+1} R^{(n-1)} \alpha_n = \sum_{m=1}^{\infty} B_{nm} \frac{\gamma z_m}{(m+1)}, \quad \text{(A 17)}$$

where

$$B_{nm} = (-1)^{n+m+1} \frac{\pi}{A_n} (2n+1) m(m+1)$$

$$\times \left[D_{(n-1),(m-1)} + \frac{Z_m}{2m+1}\left(\frac{\delta_{nm}}{\pi m(m+1)} - T_{(n-1),(m-1)}\right)\right].$$

The inverse matrix C^{-1}_{nk} may be obtained by truncating to N terms and making use of standard matrix inversion codes.

REFERENCES

Bisch, C., Lasek, A. & Rodot, H. A. 1982 Comportement hydrodynamique de volumes liquides spheriques semi-libres en apesanteur simulee. *J. Méc. Theor. Appl.* **1**, 165–183.

Collins, W. D. 1961 On some dual series equations and their application to electrostatic problems for spheroidal caps. *Proc. Camb. Phil. Soc.* **57**, 367–383.

Lamb, H. 1932 *Hydrodynamics*. Cambridge University Press.

Marston, P. 1980 Shape oscillation and static deformation of drops and bubbles driven by modulated radiation stresses – Theory. *J. Acoust. Soc. Am.* **67**, 15–26.

Miller, C. A. & Scriven, L. E. 1968 The oscillation of fluid droplets immersed in another fluid. *J. Fluid Mech.* **32**, 417–435.

Morse, P. M. & Feshbach, H. 1953 *Methods of Theoretical Physics*. McGraw-Hill.

Prosperetti, A. 1980 Normal mode analysis for the oscillations of a viscous liquid drop in an immiscible liquid. *J. Méc.* **19**, 149–182.

Rodot, H. A. & Bisch, C. 1984 Oscillations de volumes liquides semi-libres en microgravite – Experience ES326 dans Spacelab 1, *5th European Symp. on Material Sciences under Microgravity, Paper ESA SP-222*, pp. 23–29.

Strani, M. & Sabetta, F. 1984 Free vibrations of a drop in partial contact with a solid support. *J. Fluid Mech.* **141**, 233–247.

TRINH, E. & WANG, T. G. 1982 *Proc. 2nd Intl Colloq. on Drops and Bubbles. Publ.* 82–87. JPL, Pasadena (USA).

TRINH, E., ZWERN, A. & WANG, T. G. 1982 An experimental study of small-amplitude drop oscillations in immiscible liquid system. *J. Fluid Mech.* **115**, 453–474.

TSAMOPOLOUS, J. A. & BROWN, R. A. 1983 Nonlinear oscillations of inviscid drops and bubbles. *J. Fluid Mech.* **127**, 519–527.